Heat Transfer from a Plate Elevated above a Host Surface and Washed by a Separated Flow Induced by the Elevation Step

E. M. Sparrow
Fellow ASME

F. Samie
S. C. Lau

Department of Mechanical Engineering,
University of Minnesota,
Minneapolis, Minn. 55455

Wind tunnel experiments were performed to determine heat transfer coefficients and fluid flow patterns for a thermally active surface elevated above a parallel host surface. The step-like blockage associated with the elevation causes flow separation and recirculation on the forward portion of the thermally active surface. Four parameters were varied during the course of the experiments, including the angle of attack of the oncoming airflow relative to the surface, the step height, the extent of the host surface which frames the active surface (i.e., the skirt width), and the Reynolds number. Flow visualization studies, performed with the oil-lampblack technique, showed that the streamwise extent of the separation zone increases with decreasing angle of attack, with larger step heights and skirt widths, and at higher Reynolds numbers. At larger angles of attack, separation does not occur. The experimentally determined heat transfer coefficients were found to increase markedly due to the flow separation, and separation-related enhancements as large as a factor of two were encountered. The enhancement was accentuated at small angles of attack, at large step heights and skirt widths, and at high Reynolds numbers. A main finding of the study is that the separation-affected heat transfer coefficients are generally greater than those for no separation, so that the use of the latter may underestimate the heat transfer rates. For an application such as a retrofit solar collector, such an underestimation of the wind-related heat loss would yield an optimistic prediction of the collector efficiency.

Introduction

This paper is concerned with the heat transfer characteristics and related patterns of fluid flow for a plate that is inclined to an airstream, with part of the plate surface being washed by a separated, recirculating flow. The physical situation under consideration is depicted schematically in the upper diagram of Fig. 1 . As shown there, a heat transfer surface is elevated above a host surface such that the two surfaces are parallel to each other and are inclined to an airflow. The mounting arrangement of the elevated surface presents a step-like blockage to the oncoming flow. The flow attempts to climb the step but, because of its inability to turn sharp corners, separated regions, containing recirculating fluid, occur. One such separated region is situated on the forward portion of the heat transfer surface, while a second zone of separation occurs at the intersection of the step and the host surface. In general, literature information on separated, recirculating flows indicates that the corresponding heat transfer coefficients are decisively different from those for flows which move in the mainstream direction.

While the study of the aforementioned physical situation can be regarded as basic research on a complex external flow, it also bears a clear relationship to the design of flat plate solar collectors, as will now be elaborated. Flat plate collectors are highly susceptible to heat losses, as witnessed by the fact that their efficiencies are on the order of 50 percent or lower. One of the significant heat loss paths is via forced convection from the upper cover plate of the collector to the wind which passes over the collector. Consequently, heat transfer coefficients for airflow over surfaces which are geometrically similar to collector surface configurations are needed for a proper appraisal of wind-related heat losses.

The situation is particularly complex in the case of a collector that is installed on the roof of an existing building (i.e., retrofit installation). In that case, there is little likelihood that the upper surface of the collector will be flush with the surface of the roof. Rather, the collector will be mounted atop the roof, so that its upper surface is elevated above the plane of the roof. With respect to the oncoming airflow, the thus-mounted collector presents a step-like blockage to the flow.

In light of the foregoing discussion, it is evident that the configuration to be studied here serves to model the retrofit installation of a solar collector. Thus, in addition to their basic research content, the present results should have application to solar collector design.

There is no information in the solar literature about wind-related heat transfer coefficients which takes account of the elevation of the collector above a host surface, nor are there related results in the basic heat transfer literature. Until the recent past, solar texts and compendiums (e.g., [1–3]) recommended the equation $h_w = a + bV^n$ for the wind-related heat transfer coefficient, where V is the wind velocity and a, b, and n are empirical constants. This equation, based on experiments for airflow parallel to a heated plate, is actually inappropriate for solar applications. It does not take account of either the orientation of the wind vector with respect to the collector plate or of the streamwise length of the collector plate. Recent experiments [4–6] have dealt with these issues and have yielded a dimensionless

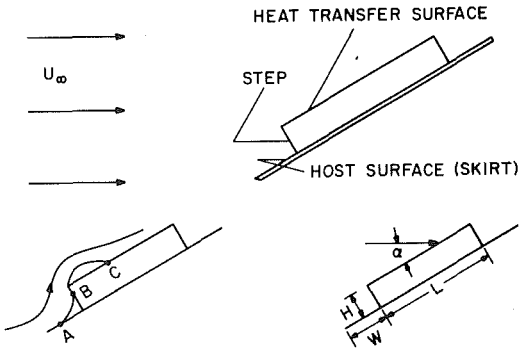

Fig. 1 Diagrams showing the physical situation, nomenclature, and perceptions of the separation zones

Contributed by the Heat Transfer Division for publication in the JOURNAL OF HEAT TRANSFER. Manuscript received by The Heat Transfer Division September 12, 1980.

correlation for h_w. However, neither the aforementioned inappropriate equation nor the new dimensionless correlation take account of the recirculating flow which washes the upper surface of an elevated collector.

Very recently [7], it was demonstrated that the use of an inappropriate wind-related heat transfer coefficient could have a marked effect on the predicted performance of a flat plate solar collector.

The present research encompassed two complementary portions, both of which dealt with the configuration pictured in Fig. 1. One of these was the determination of heat transfer coefficients for the elevated surface. The other was a flow visualization study which was focused on revealing the pattern of fluid flow adjacent to the elevated surface.

The heat transfer coefficients were determined indirectly from mass transfer measurements and by subsequent application of the well-established analogy between heat and mass transfer [8]. For the mass transfer measurements, the naphthalene sublimation technique was used. Relative to direct heat transfer measurements, the advantages of the naphthalene technique lie in the absence of extraneous losses via structure and supports, easier attainment of boundary condition uniformity, and generally higher accuracy. The heat transfer boundary condition analogous to that of the mass transfer experiments is uniform wall temperature. The flow visualization studies were performed by employing the oil-lampblack technique.

The experiments were carried out in a low-turbulence, subsonic wind tunnel, with a plate of square planform being used as the active mass transfer surface. Four parameters were varied during the course of the experiments. Three of these are geometrical parameters and are illustrated in the lower right of Fig. 1. They include: (1) the angle of attack α of the oncoming airflow relative to the plate surface, (2) the height H of the step, and (3) the width W of the portion of the host surface which frames the active mass transfer surface. Both H and W will be reported in terms of dimensionless ratios, H/L and W/L respectively, where L is the streamwise length of the elevated mass transfer surface (L was held fixed for the experiments). The fourth parameter is the Reynolds number Re. The experiments were conducted so that for fixed values of H/L, W/L, and Re, the angle of attack α was varied systematically and served as the independent variable against which the heat (mass) transfer results are plotted.

The format chosen for the presentation of the heat transfer results enables ready identification of the range of operating conditions where flow separation plays a significant role; the deviations of the separation-affected coefficients from those for separation-free flow are also clearly portrayed. The visualization studies revealed the boundary of the separated region on the active surface as well as the streamline patterns of the flow adjacent to the surface.

The Experiments

Experimental Apparatus. The mass transfer model used in the experiments is shown in pictorial view in Fig. 2. In essence, the model consists of a naphthalene-filled cavity situated atop a flat plate. The metallic portion of the model (i.e., all parts of the model aside from the naphthalene) is a one-piece unit which was machined from a single block of aluminum. As seen in the figure, the walls of the cavity frame the exposed surface of the naphthalene. The 0.117-cm (0.046-in.) thickness of the frame was the minimum that could be machined consistent with the attainment of straight walls, uniform thickness, and a smooth exposed edge. Also shown in the diagram is the 45-degree beveled leading edge of the model (i.e., the edge which thrusts forward into the airflow); the purpose of the beveling was to avoid bluntness effects.

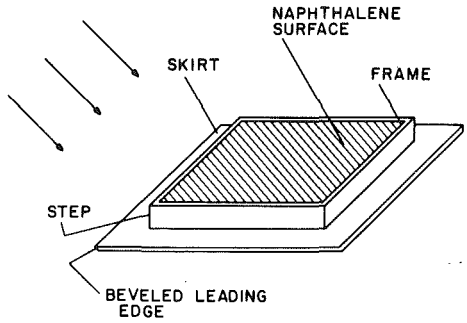

Fig. 2 Pictorial view of the mass transfer model

The dimensions of the model were chosen so as to avoid excessive blockage of the 61 × 30.5 cm (2 × 1 ft) cross section of the wind tunnel. Experience has indicated that when the blockage is small (~ three percent or less), the results of wind tunnel experiments can be applied without correction for flows in large unbounded domains. To fulfill this constraint, the base plate, the projected area of which is the blockage area, was initially fabricated as a 8.89 × 8.89 cm (3.5 × 3.5 in.) square. The elevated surface (i.e., the naphthalene surface plus the thickness of the framing walls of the cavity) was also a square, with dimensions 6.35 × 6.35 cm (2.5 × 2.5 in.) thereby leaving a 1.27 cm (0.500 in.) skirt all around. As initially fabricated, the step height was 1.27 cm (0.500 in.). The thickness of the base plate, selected to be the minimum consistent with strength and structural considerations, was 0.159 cm ($\frac{1}{16}$ in.).

As was noted in the Introduction, the step height and the skirt width were varied during the course of the investigation. With regard to the step height, it was reduced to 0.846 cm (0.333 in.) after the completion of the data runs for the initial height. Subsequently, when the runs for the second step had been completed, the height was reduced once again, this time to 0.423 cm (0.167 in.). These height reductions were accomplished by machining the edges of the cavity wall with a milling machine.

With regard to the skirt width, the visualization studies revealed that only the portion of the skirt which thrusts forward into the oncoming stream has a significant effect on the flow pattern on the mass transfer surface. Therefore, changes in width were made only for that part of the skirt. On completion of the planned data runs with the original skirt, it was removed (by milling) and replaced by a 2.54 cm (1.000 in.) skirt which was held in place by rivets which were anchored within the naphthalene cavity. A final set of runs was made with the forward skirt removed altogether.

The geometric characteristics of all the variants of the mass transfer model are listed in Table 1 in terms of the quantities H, W, and L that are defined in the lower diagram in Fig. 1. The range of the angle of attack α is also indicated in the table.

The model was mounted in the test section of the wind tunnel by means of a sting which was suspended from the upper wall of the tunnel. A swivel-type coupling situated at the forward end of the sting enabled the angle of incidence α to be set and maintained at any value between 0 and 90 deg, with the angle being read with a protractor. The

Nomenclature

c_p = specific heat
$\mathcal{D}$ = diffusion coefficient
H = step height, Fig. 1
h = average heat transfer coefficient
h^* = value of h for nonseparated flow
j = Colburn j-factor, equations (2) and (3)
j^* = j-factor value for nonseparated flow
K = average mass transfer coefficient, equation (1)
K^* = value of K for nonseparated flow
L = streamwise length of active surface
$\dot{m}$ = rate of mass transfer per unit area
Pr = Prandtl number
Re = Reynolds number, $U_\infty L/\nu$
Sc = Schmidt number
U_∞ = free stream velocity of oncoming flow
X_r = distance of reattachment line from leading edge of active surface
W = width of forward-thrusting skirt
α = angle of attack, Fig. 1
ν = kinematic viscosity
ρ = density
ρ_{nw} = naphthalene vapor density at active surface
$\rho_{n\infty}$ = naphthalene vapor density in free stream

Table 1 Geometric characteristics of the mass transfer models

H/L	W/L	α (deg)
1/5	1/5	15–60
1/7.5	1/5	15–60
1/15	1/5	15–60
1/15	1/2.5	15–60
1/15	0	15–60

coupling mated with a socket-like fixture that had been machined into the underside of the base surface of the model. The sting supported the model from the rear—the rear support being chosen to avoid disturbing the flow over the windward surfaces of the model.

Mass Transfer Surface. The naphthalene test surface was produced by a casting process utilizing a two-part metallic mold. One of the parts is the aluminum model itself, while the other is a thick, highly polished stainless steel plate. To initiate the casting process, the solid naphthalene contained in the model cavity from a prior data run is removed by melting and subsequent evaporation. Then, the model is placed face down on the stainless steel plate so that the rear surface of the base plate is up while the open end of the cavity is down (and blocked by the steel plate). A funnel is implanted in an aperture in the upfacing surface to facilitate the pouring of molten naphthalene into the cavity. Risers in the form of small diameter tubes are also implanted in holes in the upfacing surface to facilitate the escape of air displaced from the cavity by the molten naphthalene.

Once the naphthalene had solidified, the two parts of the mold were separated, exposing the naphthalene surface that had been cast against the highly polished stainless steel plate. The quality of the cast naphthalene surface was uniformly excellent—equal to that of the plate against which it was cast.

A new mass transfer surface was cast for each data run using fresh (previously unused) reagent-grade naphthalene. Once the casting had been made, the pouring aperture and the air-escape holes were carefully sealed with a pressure-sensitive tape, thereby ensuring that the test surface would be the only naphthalene surface exposed to the airflow in the wind tunnel.

A cover, made of plexiglass, was designed to fit over the entire elevated portion of the model (i.e., both the test surface and the step). When locked in place by two spring-loaded clamps which pressed the flange of the cover against the base plate, the cover served to provide an air-tight seal around the test surface. This seal served to prevent sublimation during the preparatory stage of the data run, as will be described shortly.

Instrumentation and Experimental Procedure. For the determination of the mass (heat) transfer coefficients and their correlation with the airflow, six quantities were measured for each data run. The amount of mass transferred during the course of the run was obtained from weighings of the model immediately before and immediately after the run. For the weighing, a vernier-equipped Mettler analytical balance was employed; the balance had a smallest scale division of 0.1 mg and a total weighing capacity of 200 g. The temperature of the airflow adjacent to the model was measured with an ASTM-certified 0.1°F thermometer positioned just downstream of the model. The accuracy of the thermometer was verified by comparisons with a secondary standard.

To determine the free stream velocity of the air approaching the model, a retractable impact tube was used in conjunction with a wall static tap. The impact and static pressures were conveyed via plastic tubing to the ports of a Baratron solid-state capacitance-type pressure meter capable of discriminating pressure differences to 10^{-4} mm Hg. The output of the pressure meter was read with a digital voltmeter. The impact tube–wall tap combination was checked against a Pitot tube with integral pressure taps, with a resulting agreement within one percent. For the static pressure in the test section of the wind tunnel, the Baratron was used to measure the tunnel static relative to ambient, and the ambient pressure was read from a precision barometer. The duration of the data run was read with a stop watch to within one second, while the angle of attack was set with the aid of a protractor.

As noted earlier, a new naphthalene test surface was cast for each data run. To prepare for a run, airflow was initiated in the wind tunnel, and the controls were set to yield the desired Reynolds number. The tunnel was operated in the open-circuit mode, with air being drawn from the building and exhausted to the outdoors. This mode of operation ensured that the air approaching the model would be free of naphthalene vapor and, since the fan is positioned downstream of the test section, there was no preheating of the air.

The tunnel was allowed to operate for about an hour to attain steady state. At that point of time, the model was weighed and the cover applied and clamped in place. The thus-capped model was then affixed on the sting in the wind tunnel and the angle of attack α was set. Previous experience had demonstrated that the capped model achieved a steady temperature equal to that of the flowing air within a half hour. During the equilibration period, the air velocity and temperature were carefully monitored for constancy. Then, after the passage of a half hour (or longer) the impact tube was retracted, and the data run proper was initiated by uncapping the model and starting the stop watch.

Temperatures were read and recorded at frequent intervals during the data run. The duration of the run was selected so that the amount of mass transfer could be measured accurately while limiting the average recession of the surface to 0.0025 cm (0.001 in.). Depending on the operating conditions, 100 to 200 mg were sublimed, and run times ranged from 20 to 75 min.

To conclude the run, the wind tunnel hatch was opened, and the model cap was applied and clamped. The mass of the model was immediately measured. Before the tunnel was turned off, a calibration procedure was executed to correct for any ambiguities in mass transfer during the model's installation in and removal from the wind tunnel. The airspeed was also measured prior to shutdown.

Flow Visualization. As noted earlier, the oil-lampblack technique was employed to enable visualization of the flow field adjacent to the elevated surface. Lampblack is a very fine black powder now primarily available as an ingredient of paint. It mixes readily with oil, and the mixture, when brushed on a surface, produces a smooth, glossy-black coating. The fluidity of the mixture can be regulated by the selection of the viscosity of the oil and by the proportions of the oil and the lampblack powder. These proportions also have a significant effect on the degree of definition of the flow pattern that can be achieved with the method. The degree of fluidity of the mixture is an especially relevant factor when the flow adjacent to an inclined surface is to be visualized, as is the case in the present investigation. In such a situation, the mixture will sag under the action of gravity, unless it is sufficiently stiff.

The general procedure for using the technique is to brush the oil-lampblack mixture on a surface and then to expose the surface to the airflow whose characteristics are to be studied. Ideally, under the action of the shear stresses exerted by the flow, the mixture will move along the surface, following the paths of the fluid particles that pass adjacent to the surface. These path lines will appear as streaks on the surface. In regions of low shear stress (e.g., at separation, reattachment, or stagnation), the mixture will remain stationary, so that such regions show themselves as black streak-free zones on the surface.

For all of the visualization runs, the elevated surface was coated with white, plasticized contact paper in order to obtain the highest possible contrast for the black streak lines and the black low-shear zones. In order to attain the clearest possible patterns, the bulk of the visualization work was performed at the highest Reynolds number investigated (~70,000), which also corresponded to the highest shear stress. Some observations made at lower Reynolds numbers will also be reported.

Results and Discussion

The presentation of results will begin with the information obtained from the flow visualization studies, with the heat (mass) transfer results to follow.

Flow Visualization Results. To provide guidance for the interpretation of the visualization results, attention will be directed to the diagram at the lower left of Fig. 1. This diagram shows a perception

of the expected separation zones associated with the presence of the step. These separation zones are created because the flow is unable to turn the sharp corners at both the bottom and top of the step. Within each separation zone, there is a recirculating flow.

Of particular interest is the point C where the mainflow reattaches to the elevated surface. Downstream of C, the fluid adjacent to the surface moves in the streamwise direction, whereas upstream of C (within the separation bubble), the fluid adjacent to the surface moves upstream. Thus, C is a point of zero shear, and it should appear as a dark spot in the oil-lampblack visualization (actually as a line when the plate is viewed head-on rather than from the side). Similarly, points A and B, which respectively correspond to separation and reattachment, should also appear as black lines.

These expectations were actually realized during the visualization runs. All three lines were observed, but primary attention was focused on the reattachment at C since the heat (mass) transfer is directly affected by the extent of the separated zone which washes the forward part of the elevated surface.

Illustrative flow-visualization photographs showing head-on views of the elevated surface are presented in Fig. 3. These photographs correspond to the highest Reynolds number of the experiments (70,000), to the intermediate step height (H/L = 1/7.5), and to the intermediate skirt width (W/L = 1/5). In the upper row, the successive photographs (left to right) are for angles of attack α of 15, 20 and 30 deg, while the lower photographs are for α values of 40, 45, and 50 deg. These photographs show the traces of the streamlines adjacent to the surface as well as the reattachment line. In some of the photographs, extraneous black regions caused by sagging of the oil-lampblack mixture are visible.

By inspection of Fig. 3, it is seen that the reattachment line moves forward toward the leading edge and finally disappears as the angle of attack increases. This decrease in the size of the separated region with angle is altogether reasonable and reflects the decrease of the projected step height as seen by the oncoming flow. The reattachment line is more or less parallel to the leading edge, indicating a nearly two-dimensional flow pattern in the neighborhood of reattachment. Indeed, in the recirculation region, the streamlines are straight and parallel. Even downstream of reattachment, the flow is nearly two-dimensional except near the side edges of the surface. As the size of the separation zone shrinks with increasing angle, three-dimensionality becomes more evident.

As noted earlier, the bulk of the flow visualization runs were made at the highest Reynolds number (~70,000) because the relatively high shear stresses provided the most sharply etched flow pattern traces. For this Reynolds number and for all step heights and skirt widths investigated, the reattachment distance (i.e., distance between the leading edge of the elevated surface and the reattachment line) was measured. The reattachment distance, to be termed X_r, is a direct index of the size of the separated region. It was measured directly from the visualization patterns on the model surface (not from photographs).

Dimensionless reattachment distances X_r/L are plotted in Figs. 4 and 5 as a function of the angle of attack α. Figure 4 conveys results for parametric values of the step height H/L at a fixed skirt width W/L = 1/5, whereas Fig. 5 is for a fixed step height H/L = 1/15 with the skirt width serving as the parameter. Turning first to Fig. 4, it is seen that the trend of reattachment distance decreasing with angle, as evidenced earlier by the photographs of Fig. 3, is reaffirmed. At the smaller angles of attack, the reattachment distance is quite sensitive to the step height, increasing as the step height increases. On the other hand, for angles of 30 deg and larger, the reattachment distance is more or less independent of the height of the step. At angles of 50 deg

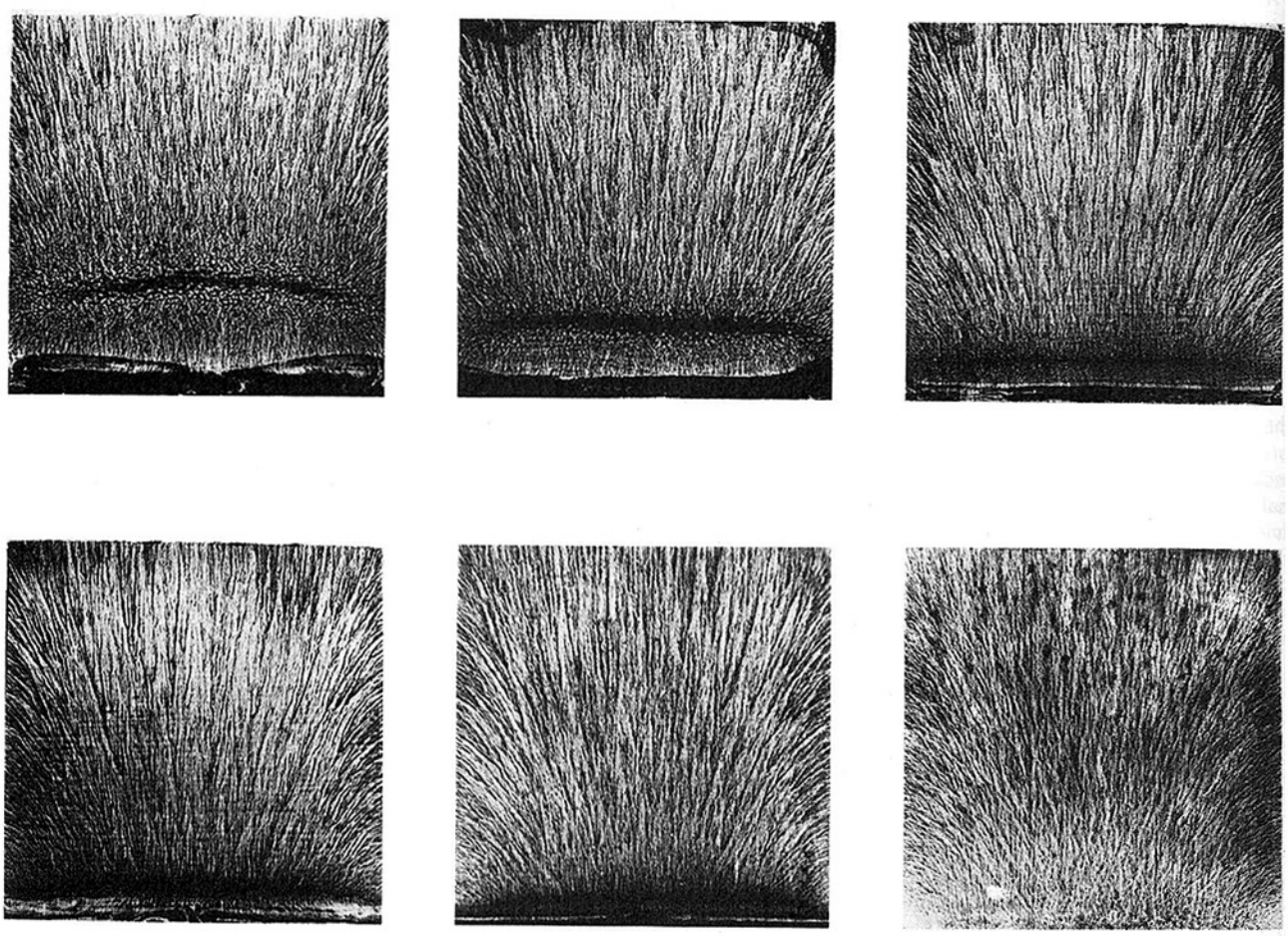

Fig. 3 Illustrative flow-visualization photographs; Re~ 70,000, H/L = 1/7.5, and W/L = 1/5. Upper row (left-to-right), α = 15, 20, and 30°; lower row (left-to-right), α = 40, 45, and 50°

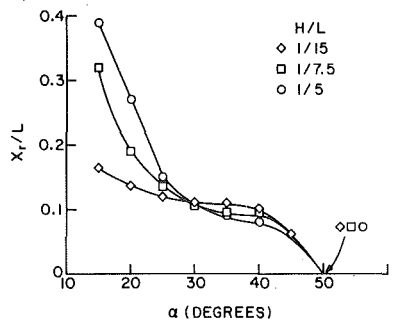

Fig. 4 Reattachment distances for various step heights at a skirt width W/L = 1/5 and Re ~ 70,000

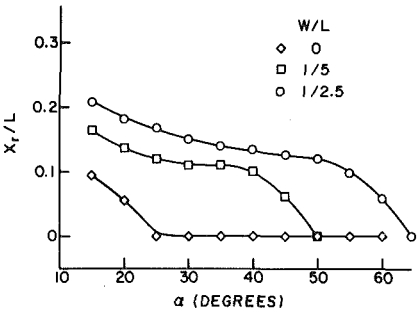

Fig. 5 Reattachment distances for various skirt widths at a step height H/L = 1/15 and Re ~ 70,000

or larger, separation could not be detected.

As a supplement to the data presented in Fig. 4, additional visualization runs were performed over a range of Reynolds numbers at various fixed angles of attack. In general, there was a tendency for the reattachment distance to increase with the Reynolds number, rather rapidly at first and then very slowly. The X_r/L values of Fig. 4 are more or less applicable for Reynolds numbers in the range 45,000 to 70,000.

The results of Fig. 5 show that the reattachment distance is quite sensitive to the width of the skirt that thrusts forward from the base of the step. In general, the greater the skirt width, the larger the reattachment distance. In addition, separation persists at larger angles of attack for wider skirts. For the no-skirt case, the reattachment distance is generally small, and separation does not occur at angles of 25 deg or greater.

Brief observations will be made about points A and B (lower left, Fig. 1), which are the anchor points of the separation zone at the foot of the step. Point A moves slowly forward toward the step as the angle of attack increases. At angles of 40 deg and larger, a stagnation line first appears on the skirt and, as the angle increases, the stagnation line and the separation line markedly interact. Point B, which is situated at mid-height at low angles, moves up the step as the angle increases and finally disappears. This disappearance coincides with the condition that no separation occurs on the elevated surface.

With regard to the relation of the visualization results to heat (mass) transfer, it may be expected that the larger the separation zone, the greater the transfer. This expectation is based on the belief that at the Reynolds numbers investigated, the separated region will contain a vigorously recirculating fluid. Consequently, high rates of transfer are expected at low angles of attack, high steps, wide skirts, and high Reynolds numbers.

Dimensionless Heat (Mass) Transfer Parameters. The interchangeability of heat and mass transfer results, which has been noted at various points throughout the paper, will now be formalized. First, a mass transfer coefficient K is defined as

$$K = \dot{m}/(\rho_{nw} - \rho_{n\infty}) \tag{1}$$

where $\dot{m}$ is the rate of mass transfer per unit surface area, and ρ_{nw} and $\rho_{n\infty}$ are the densities of naphthalene vapor at the mass transfer surface and in the free stream. A convenient dimensionless version of the mass transfer coefficient is given by the Colburn j-factor

$$j = (K/U_\infty)\mathrm{Sc}^{2/3} \tag{2}$$

in which U_∞ is the free stream velocity and Sc is the Schmidt number (analogous to the Prandtl number). There is also a j-factor for heat transfer given by

$$j = (h/\rho c_p U_\infty)\mathrm{Pr}^{2/3} \tag{3}$$

According to the Colburn Analogy, the j values for heat and mass transfer are equal at any given value of Reynolds number.

The exponent 2/3 of Pr and Sc in equations (2) and (3) bears some discussion in view of the fact that for certain operating conditions, a portion of the plate surface is covered by a zone of flow separation. Within the knowledge of the authors, the effect of Pr (or Sc) on heat (mass) transfer coefficients in separated flows has not yet been definitively correlated. There is evidence, however, that the 2/3 power may not be too far off the mark. In [9], the Nusselt number for a cylinder in crossflow (a situation where about half the surface is washed by a separated flow) was correlated with $\mathrm{Pr}^{0.37}$, which corresponds to $(h/\rho c_p U_\infty)\mathrm{Pr}^{0.63}$ = constant at a given value of Reynolds number. In the range of Pr or Sc between 0.7 and 2.5, which encompasses the Prandtl number for heat transfer in air and the Schmidt number for naphthalene diffusion in air, there is little difference between a $\mathrm{Pr}^{2/3}$ dependence or a $\mathrm{Pr}^{0.63}$ dependence. However, to minimize the issue of which exponent is appropriate, most of the results are presented in a ratio form which eliminates the presence of the thermophysical properties.

The j-factor for mass transfer was evaluated from equations (1) and (2) by using the experimental data. To determine $\dot{m}$, the change in mass during a data run was divided by the duration of the run and the mass transfer surface area. The determination of ρ_{nw} involves a two-step process. First, the naphthalene vapor pressure p_{nw} at the wall was evaluated from the Sogin relation [10] with the measured temperature as input. Then, with p_{nw} and with the temperature, ρ_{nw} was calculated from the perfect gas law. With regard to $\rho_{n\infty}$, the complete absence of naphthalene vapor in the free stream gives $\rho_{n\infty}$ = 0.

The Schmidt number appearing in equation (2) was evaluated from its definition

$$\mathrm{Sc} = \nu/\mathcal{D} \tag{4}$$

Since the naphthalene vapor concentration is minute, the kinematic viscosity can be taken as that of pure air. The diffusion coefficient $\mathcal{D}$ was calculated from Skelland's formula [11]. For the operating conditions of the experiments, Sc ~2.55.

The Reynolds number, which served to parameterize the results, was defined as

$$\mathrm{Re} = U_\infty L/\nu \tag{5}$$

in which L is the streamwise length of the test surface.

Heat (Mass) Transfer Results. To help identify a format which would be most effective in displaying the effects of flow separation, working graphs were prepared in which j was plotted as function of the angle of attack α for a fixed Reynolds number and for fixed geometry. It was observed from these graphs that j varied with α in the range of small and intermediate α, but that j was essentially a constant at larger α. This latter behavior confirms a prior finding [4, 6] that j is a very weak function of α in separation-free flow. It was further observed that in the range where j was nearly independent of α, it was also relatively insensitive to the specifics of the model geometry (i.e., step height, skirt width).

These characteristics suggested a presentation format that is exemplified by any one of Figs. 6 to 9. Consider, for example, Fig. 8. This figure corresponds to a fixed Reynolds number, Re = 50,000, and to a fixed skirt width, W/L = 1/5. In the figure, j/j^* is plotted as a function of the angle of attack α for parametric values of the step height H/L = 1/5, 1/7.5, and 1/15. The quantity j^* is equal to the average of the j values that fall in the α-independent portion of the data range. Aside from the secondary effect of geometry in the α-independent regime, j^* corresponds to the j value for separation-free flow at the Reynolds number in question.

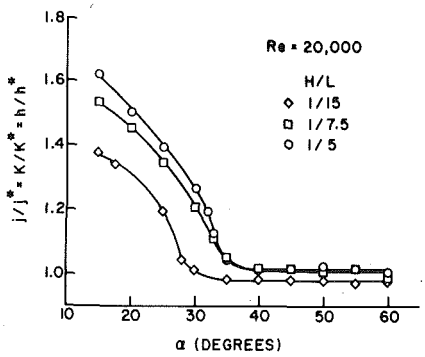

Fig. 6 Heat (mass) transfer coefficients for various step heights at a skirt width W/L = 1/5; Re = 20,000 and j^* = 0.00603

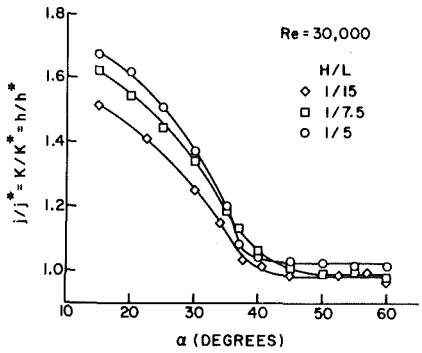

Fig. 7 Heat (mass) transfer coefficients for various step heights at a skirt width W/L = 1/5; Re = 30,000 and j^* = 0.00492

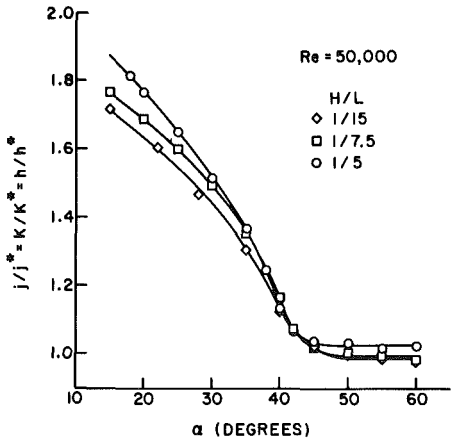

Fig. 8 Heat (mass) transfer coefficients for various step heights at a skirt width W/L = 1/5; Re = 50,000 and j^* = 0.00379

In light of the foregoing, it is evident that deviations of j/j^* from unity are indicative of the effect of flow separation on the heat transfer coefficient. Furthermore, since j and j^* correspond to the same Reynolds number and to the same thermophysical properties, it follows that $j/j^* = K/K^* = h/h^*$. The ordinates of the figures have been labeled to reflect these equalities.

Figures 6 to 9 convey results for j/j^* versus α for a fixed skirt width W/L = 1/5, with each successive figure corresponding to a fixed Reynolds number equal to 20,000, 30,000, 50,000, and 70,000. The data in each figure are parameterized by the step height H/L, and curves have been faired through the data to provide continuity.

The striking feature of these figures is the large values of j/j^* that are encountered as the angle of attack decreases. These increases in j/j^* can be directly attributed to the enlargement of the separated region that was displayed in Figs. 3 to 5. For the operating conditions of the experiments, separation-induced increases in heat transfer coefficient of almost a factor of two are in evidence.

As shown in the figures, the highest heat transfer coefficients are attained at the smallest of the investigated angles of attack, α = 15 deg. As α increases, the transfer coefficient decreases monotonically

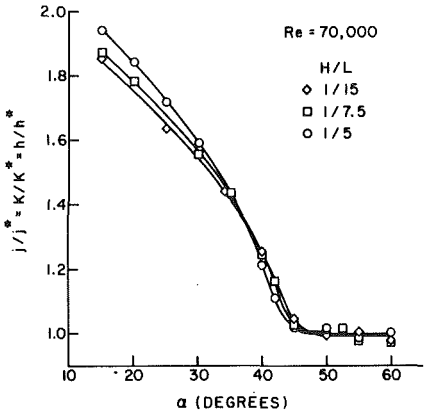

Fig. 9 Heat (mass) transfer coefficients for various step heights at a skirt width W/L = 1/5; Re = 70,000 and j^* = 0.00329

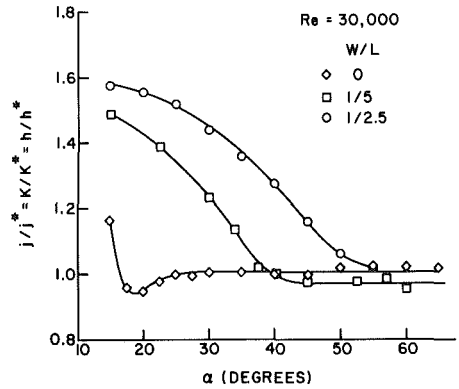

Fig. 10 Heat (mass) transfer coefficients for various skirt widths at a step height H/L = 1/15; Re = 30,000 and j^* = 0.00495

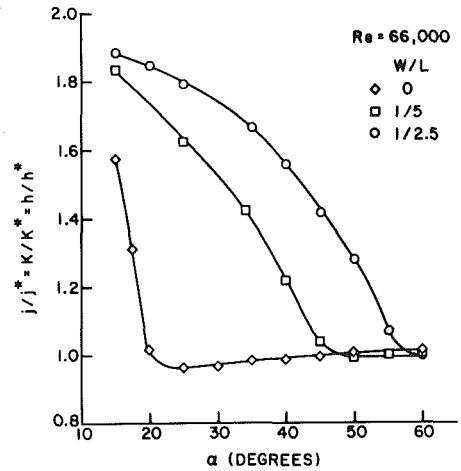

Fig. 11 Heat (mass) transfer coefficients for various skirt widths at a step height H/L = 1/15; Re = 66,000 and j^* = 0.00337

and levels off to the separation-free value, with the leveling-off taking place in the α range 35–45 deg, depending on the operating conditions.

With regard to step height, higher steps give rise to progressively greater enhancement of the heat transfer coefficient at those α values where there is significant enhancement. However, at lower enhancements, there is some crossing of the curves for the various step heights, but in that range the enhancements caused by the different step heights are not very different. These trends with step height tend to reflect the variation of the reattachment distance with step height as portrayed in Figs. 4 and 5.

From a careful examination of Figs. 6 to 9, a number of significant Reynolds-number-related effects can be identified. First of all, the general level of enhancement increases as the Reynolds number in-

creases. This is due to the increased vigor of the recirculating flow in the separation zone. Second, there is a diminished sensitivity to variations of step height at higher Reynolds numbers. Finally, enhancement persists to higher angles of attack at larger Reynolds numbers. Thus, for example, at Re = 70,000, enhancement persists to α = 45 deg, while at Re = 20,000, enhancement has effectively ceased at 35 deg, for the higher steps and at 25–30 deg for the lowest step.

Attention may now be turned to the effect of skirt width on the heat transfer coefficient, with the step height being held fixed at H/L = 1/15. These results are presented in Figs. 10 and 11, which correspond respectively to Re = 30,000 and 66,000. In each figure, j/j^* is plotted as a function of α for parametric values of the forward-thrusting skirt width W/L = 1/2.5, 1/5, and 0. The results shown in these figures convey a clear message, namely, that the separation-related enhancement of the heat transfer coefficient is markedly affected by the skirt width.

Not only is the magnitude of j/j^* significantly affected by skirt width, but also is the range of angles of attack at which enhancement occurs. Both the magnitude of the enhancement and the angles to which enhancement persists are increased as the skirt width becomes greater.

The curves for the two non-zero skirt widths have similar shapes. It is interesting to note that there is a definite tendency for these curves to come together at smaller angles as well as at larger angles. The enhancement effects for the wider of the two skirts persist to angles that are 10–15 deg larger than for the narrower skirt.

The characteristics evidenced by the no-skirt case are altogether different from those for the finite-width skirts. First of all, there is no significant enhancement of the heat transfer coefficient for angles greater than 15–20 deg. Furthermore, an undershoot is in evidence at lower angles, whereby the heat transfer coefficient falls slightly below the large-angle separation-free value.

It is not surprising that there are such different trends when a skirt is absent and when a skirt is present. These differences can be attributed to differences in the respective flow fields. Thus, for example, the separated region at the foot of the step (between points A and B, Fig. 1, lower left) is no longer present when there is no skirt. Furthermore, a stagnation line which would otherwise lie in the skirt may shift to the step when the skirt is absent.

In common with the trends of earlier figures, the effect of higher Reynolds numbers, as evidenced in Figs. 10 and 11, is to increase the degree of enhancement and to extend the range of angles where enhancement occurs.

Concluding Remarks

The research reported here was aimed at determining heat transfer coefficients for a thermally active surface elevated above a host surface. Supplementary flow visualization experiments, intended to provide insights into the patterns of fluid flow adjacent to the surface, were also carried out.

The visualization studies demonstrated the presence of a region of flow separation which blankets the forward part of the elevated surface. Fluid recirculation within the separated region was inferred from the streak lines on the surface. The streamwise extent of the separated region was found to increase with decreasing angle of attack. On the other hand, at larger angles of attack, separation does not occur. Separated regions of greater extent were encountered at larger step heights and for greater widths of the skirt which thrusts forward into the flow. There is also a tendency toward larger separated regions at higher Reynolds numbers. Since, at the Reynolds numbers investigated, the separation zone contains vigorously recirculating fluid, larger separated regions give rise to higher heat transfer coefficients.

At a fixed Reynolds number and for fixed geometry (i.e., fixed step height and skirt width), the heat transfer coefficient increases monotonically with decreasing angle of attack. Separation-related enhancements of the heat transfer coefficient as large as a factor of two were encountered. At larger angles of attack, where there is no flow separation, the heat transfer coefficient is essentially independent of angle and of geometry.

Higher steps give rise to progressively greater heat transfer enhancement at angles where there is significant enhancement. The degree of enhancement is markedly increased as the skirt width increases and, in addition, the enhancement persists to larger angles of attack. In the absence of a skirt, there is very little enhancement.

The Reynolds number plays a significant role in the separation-induced enhancement. The degree of enhancement is greater and enhancement persists to larger angles at higher Reynolds numbers. On the other hand, with increasing Reynolds number the heat transfer coefficients become less sensitive to variations in step height.

With regard to applications, it may be concluded that the use of literature information for non-separated-flow heat transfer coefficients will generally provide a low estimate of the surface heat transfer rate. For solar collectors, such a low estimate will yield an optimistic prediction of the collector efficiency.

As a final observation, it should be pointed out that a wind tunnel is not able to model, in all details, the fluid flow conditions that are encountered in the outdoor environment, e.g., unsteadiness and turbulence characteristics. On the other hand, owing to the variability of the outdoor environment, it is unrealistic to think in terms of a universal set of fluid flow conditions for solar collectors (the specification of the mean wind speed does not characterize unsteadiness or turbulence). Thus, model experiments of any kind, whether performed in a wind tunnel or outdoors, can only approximate any particular solar collector application. While it is well to keep such concerns in mind, it is still necessary to employ the results of model experiments for solar collector design. In this light, the present results merit consideration for incorporation into solar collector design calculations.

Acknowledgment

This research was performed under the auspices of the American Society of Heating, Refrigerating, and Air-Conditioning Engineers.

References

1. Duffie, J. A., and Beckman, W. A., *Solar Energy Thermal Processes*, Wiley, New York, 1974, p. 83.
2. Jordan, R. C. and Liu, B. Y. H., eds., *Application of Solar Energy for Heating and Cooling of Buildings*, ASHRAE, New York, 1977, Chapter 8.
3. Krieth, F., and Krieder, J. F., *Principles of Solar Engineering*, McGraw-Hill, New York, 1978, p. 139.
4. Sparrow, E. M., and Tien, K. K., "Forced Convection at an Inclined and Yawed Flat Plate—Application to Solar Collectors," ASME JOURNAL OF HEAT TRANSFER, Vol. 99, 1977, pp. 507–512.
5. Tien, K. K., and Sparrow, E. M., "Local Heat Transfer and Flow Field Characteristics for Airflow Oblique or Normal to a Flat Plat," *International Journal of Heat and Mass Transfer*, Vol. 22, 1979, 349–360.
6. Sparrow, E. M., Ramsey, J. W., and Mass, E. A., "Effect of Finite Plate Width on Heat Transfer and Fluid Flow about an Inclined Rectangular Plate," ASME JOURNAL OF HEAT TRANSFER, Vol. 101, 1979, pp. 199–204.
7. Ramsey, J. W., and Charmchi, M., "Variances in Solar Collector Performance Predictions due to Different Methods of Evaluating Wind Heat Transfer Coefficients," ASME JOURNAL OF HEAT TRANSFER, Vol. 102, 1980, pp. 766–768.
8. Eckert, E. R. G., "Analogies to Heat Transfer Processes," in *Measurements in Heat Transfer*, E. R. G. Eckert and R. J. Goldstein, eds., Hemisphere, Washington, 1976.
9. Zukauskas, A., "Heat Transfer from Tubes in Crossflow," in *Advances in Heat Transfer*, Vol. 8, Academic Press, New York, 1972, pp. 93–160.
10. Sogin, H. H., "Sublimation from Disks to Air Streams Flowing Normal to their Surfaces," *Trans. ASME*, Vol. 80, 1958, pp. 61–69.
11. Skelland, A. H. P., *Diffusional Mass Transfer*, Wiley, New York, 1974, p. 51.